

Available online at www.sciencedirect.com

ScienceDirect

journal homepage: www.elsevier.com/locate/AJPS

Original Research Paper

Chondroitin sulfate-mediated albumin corona nanoparticles for the treatment of breast cancer

Tiantian Tan^a, Qin Yang^{a,b,*}, Dan Chen^a, Juan Zhao^{a,c}, Ling Xiang^a, Jiaying Feng^a, Xu Song^a, Yao Fu^a, Tao Gong^{a,*}

^a Key Laboratory of Drug-Targeting and Drug Delivery System of the Education Ministry, Sichuan Engineering Laboratory for Plant-Sourced Drug and Sichuan Research Center for Drug Precision Industrial Technology, West China School of Pharmacy, Sichuan University, Chengdu, 610064, China

^b School of Pharmacy, North Sichuan Medical College, Nanchong 637100, China

^c Departments of Pharmacy, Mianyang Hospital of Traditional Chinese Medicine, Mianyang 621000, China

ARTICLE INFO

Article history:

Received 16 November 2020

Revised 8 February 2021

Accepted 10 March 2021

Available online 20 April 2021

Keywords:

Chondroitin sulfate

Bovine serum albumin

Self-assembly

Doxorubicin

Cancer therapy

ABSTRACT

Chondroitin sulfate-mediated albumin corona nanoparticles were readily prepared without any chemical reaction, and their active tumor targeting and therapeutic effects were examined. Negatively charged chondroitin sulfate (CS) and positively charged doxorubicin (DOX) self-assembled into nanoparticles (CS-DOX-NPs) via electrostatic interactions. Bovine serum albumin (BSA) was then adsorbed on the surface of CS-DOX-NPs to form albumin corona nanoparticles (BC-DOX-NPs) protected from endogenous proteins. Due to the dual effect of BSA and CS, BC-DOX-NPs interacted with the gp60, SPARC and CD44 receptors on tumor cells, facilitating their rapid and efficient transcytosis and improving their accumulation and uptake within tumor tissues. The simultaneous presence of BSA and CS also allowed BC-DOX-NPs to target CD44 efficiently, leading to greater cellular uptake and cytotoxicity against 4T1 cells than CS-DOX-NPs or free DOX. Intravenous injection of BC-DOX-NPs into orthotopic 4T1 tumor-bearing mice led to greater drug accumulation at the tumor site than with CS-DOX-NPs or free DOX, resulting in significant inhibition of tumor growth and lower exposure of major organs to the drug.

© 2021 Shenyang Pharmaceutical University. Published by Elsevier B.V.

This is an open access article under the CC BY-NC-ND license

(<http://creativecommons.org/licenses/by-nc-nd/4.0/>)

1. Introduction

Chondroitin sulfate (CS) is a biocompatible, biodegradable anionic glycosaminoglycan with low toxicity consisting of

repeating disaccharide units of glucuronic acid and N-acetyl galactosamine. CS, a part of the extracellular matrix, has been clinically approved for wound dressings and used for adjuvant treatment of joint pain and atherosclerosis. CS and its proteoglycans have shown strong affinity for CD44

* Corresponding authors.

E-mail addresses: qinyang201@163.com (Q. Yang), gongtaoy@126.com (T. Gong).

Peer review under responsibility of Shenyang Pharmaceutical University.

and P-selectin receptors [1], which play an important role in inhibiting tumor angiogenesis and metastasis and in promoting tumor cell apoptosis [2–4]. In particular, CD44 is a membrane protein involved in tumor growth and metastasis [5,6], and is highly expressed on the surface of various cancer cells, such as breast, prostate and colon cancer cells [7–9], making it a well-established tumor targeting receptor.

CS bears many carboxyl and sulfonyl groups, which can be easily chemically modified for various applications. For instance, a chondroitin sulfate A–polyethylene glycol conjugate was synthesized and adsorbed on the surface of docetaxel crystals, affording nanocrystals with improved stability, long circulation and CD44 targeting ability [10]. Additionally, phenylboronic acid-functionalized chondroitin sulfate A nanoparticles were prepared to target tumors and release drugs in response to the acidic tumor microenvironment. [11]. Although these derivatives can be used to formulate targeted delivery systems, they still have several drawbacks such as low biocompatibility, safety issues with synthetic materials and incomplete elimination of toxic molecules during the reactions. Furthermore, once injected into circulation, the nanoparticle surface can be shielded by endogenous proteins, which interferes with the ability of targeting ligands to bind their cognate receptors, thus reducing targeting efficiency [12,13].

Albumin is commonly used to formulate various nanoparticles [14–16], which show good biocompatibility, low immunogenicity, good biodegradability and other desirable properties [17–19]. Albumin can also bind to the gp60 receptor, a glycoprotein expressed on the surface of endothelial cells; in this way, albumin can help nanoparticles cross the endothelial barrier and penetrate into tumors [20]. Moreover, albumin interacts with the so-called “secreted protein acidic and rich in cysteine” (SPARC), allowing it to accumulate at the tumor, where it serves as an energy source [17,20,21].

In this study, we aimed to prepare self-assembled CS-based nanoparticles without any chemical modification. Doxorubicin (DOX) was used as a model drug because of its excellent antitumor activity [22]. Commercially available DOX·HCl was desalted to expose its free amino groups, then it was combined with the negatively charged CS to form CS-DOX-NPs by electrostatic interactions. Given that CS has good affinity for various proteins, such as Neisseria heparin binding antigen (NHBA) [23] and albumin [24,25], we used bovine serum albumin (BSA) to generate a protective protein corona on the CS-DOX-NP surface, forming CS-mediated albumin corona nanoparticles (BC-DOX-NPs). In this way, BC-DOX-NPs were prepared via a stepwise method based on the electrostatic interaction between positive DOX and negative CS and the strong affinity between glycosaminoglycans and proteins (Fig. 1). The rationale of this approach was that after intravenous administration, BC-DOX-NPs would bind to the gp60 receptor on the surface of tumor vascular endothelial cells and activate the caveolin-1 protein. Then the nanoparticles would be transcytosed across endothelial cells. Finally, the nanoparticles would bind to SPARC and CD44 receptors on cancer cells to accumulate in the tumor interstitium and be efficiently taken up by other tumor cells.

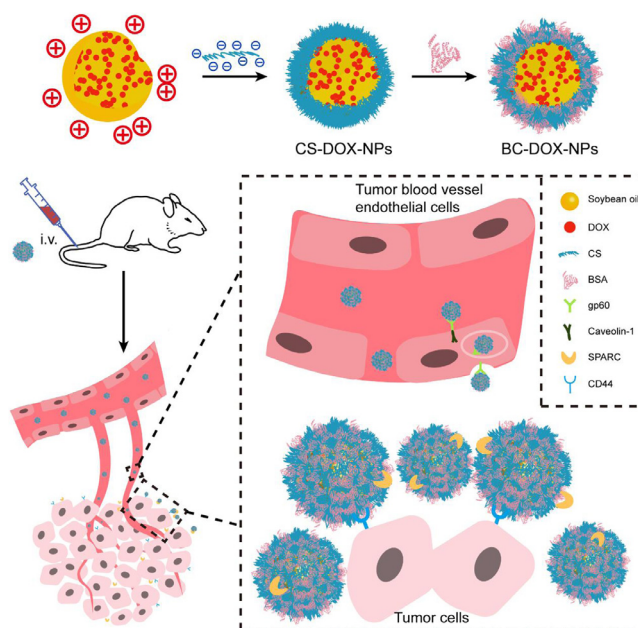


Fig. 1 – Schematic illustration showing of BC-DOX-NPs for transporting and exerting therapeutic effects in vivo. Soybean oil as hydrophobic core was used to promote DOX aggregation to form a positively charged core, and the negatively charged polysaccharide chain CS was entangled with the core during agitation (CS-DOX-NPs). BSA adsorbed on the CS-DOX-NPs surface forming BC-DOX-NPs and formed protein corona on the surface of nanoparticles. Meanwhile some CS were exposed alternately with BSA. BSA could reduce the interference of endogenous proteins on BC-DOX-NPs. In addition, the binding of BSA to gp60 on endothelial cells activates the cytoplasmic protein caveolin-1, which causes BC-DOX-NPs to cross the endothelial barrier in vesicles. BC-DOX-NPs is accumulated in tumor stroma due to the binding of BSA and SPARC, and targets to tumor cells thanks to the interaction of CS and CD44. (For interpretation of the references to colour in this figure legend, the reader is referred to the web version of this article.)

2. Materials and methods

2.1. Materials

CS was purchased from Aladdin biochemical technology Co., Ltd. (Shanghai, China); Doxorubicin hydrochloride was purchased from Meilun Biotechnology (Dalian, China); BSA (Albumin Bovine V) was purchased from BioFroxx (Einhausen, Germany); Soybean oil for injection was purchased from Yuanye Bio-Technology Co., Ltd. (Shanghai, China); Solutol HS15 was purchased from BASF (Ludwigshafen, Germany); 3-(4,5-Dimethyl-2-thiazolyl)-2,5-diphenyl-2H-tetrazolium bromide (MTT), 4,6-diamidino-2-phenylindole (DAPI), monensin sodium and genistein were purchased from J&K Scientific Ltd.; Mouse antibodies including anti-CD44, FITC anti-CD44 and Rhodamine-labeled secondary

antibodies were purchased from Affymetrix eBioscience (San Diego, USA). rabbit anti-CD31 antibody and Alexa Fluor 647 conjugated goat anti-rabbit IgG were purchased from Abcam (Cambridge, UK). Other reagents were analytical or HPLC grade and purchased commercially.

2.2. Preparation of BC-DOX-NPs and CS-DOX-NPs

DOX·HCl (20 mg), 500 µl ammonia (12.5 ppm) and 600 µl soybean oil for injection were mixed in 10 ml ethanol and sonicated in a water bath for 20 min to obtain suspension A. 33.6 mg CS (MW 113 kDa), 125 mg HS-15 were dissolved in 20 ml deionized water to obtain solution B. Suspension A was added dropwise to solution B and the mixture was stirred at room temperature for 1 h. The suspension was sonicated for 10 min (250 W), and then it was homogenized using high pressure homogenizer (1100 bar for 2 min) to obtain uniform nanoparticles. The final suspension with a volume of 5 ml was obtained after removing the ethanol using rotary evaporation. Adding deionized water to a constant volume of 15 ml to obtain CS ion-pairing nanoparticles (CS-DOX-NPs). 62.7 mg BSA was dissolved in 7 ml CS-DOX-NPs and stirred at room temperature for 1 h to obtain BC-DOX-NPs. All formulations were filtered through 0.22 µm sterile filter and stored at 4 °C.

2.3. Fluorescence spectroscopy of BSA

To further demonstrate the binding between BSA and CS-DOX-NPs, we recorded the fluorescence spectra of BSA, BC-DOX-NPs and CS-DOX-NPs using a spectrophotometer (RF6000, Shimadzu, Kyoto, Japan). The concentration of BSA or BC-DOX-NPs is 100 µg/ml and the concentration of DOX is 10 µg/ml. The fluorescence emission spectra were recorded at 25 °C in range of 200–600 nm at an excitation wavelength of 280 nm. We also recorded the fluorescence spectra of BC-DOX-NPs (BSA, 100 µg/ml) with different mass ratios of BAS to CS (1:0.167, 1:0.125, 1:0.100, 1:0.067). These fluorescence emission spectra were recorded at 25 °C in range of 290–500 nm at an excitation wavelength of 280 nm.

2.4. Cellular uptake

We examined cellular uptake of BC-DOX-NPs and CS-DOX-NPs by flow cytometry (FCM) and CLSM. For flow cytometry, B16F10 and 4T1 cells (1×10^5 cells per well) were seeded in 12-well plates. After 24 h, cells were treated with free DOX, BC-DOX-NPs and CS-DOX-NPs with DOX concentration at 5 µg/ml for 1, 2 and 4 h, respectively. Afterward, the cells were trypsinized, washed twice with PBS, and resuspended in 0.5 ml PBS. Mean fluorescence intensity and positive rate of cells were measured by flow cytometry. For CLSM, 4T1 cells were seeded on coverslips 24 h before treatment with free DOX, BC-DOX-NPs and CS-DOX-NPs. After 2 h and 4 h incubation, cells were rinsed thrice with cold PBS, fixed with 4% paraformaldehyde for 15 min, stained with DAPI for 10 min and observed by CLSM.

To prove that the cell uptake of nanoparticles is due to CD44 receptors, we blocked the receptors on 4T1 and B16F10 cells and examined uptake by flow cytometry. Briefly, cells were seeded in 12-well plates and precultured free media without or with 10 mg/ml CS for 1 h. After

1 h, cells were incubated with free DOX, BC-DOX-NPs and CS-DOX-NPs for 2 h, washed and resuspended in PBS for analysis.

2.5. Intracellular localization under CLSM

The CD44 location of BC-DOX-NPs and CS-DOX-NPs was studied in 4T1 cells by confocal laser scanning microscopy (CLSM) (TCS SP5, leica, Germany). Cells (1×10^4) were seeded on round glass coverslips overnight and incubated with free DOX, BC-DOX-NPs and CS-DOX-NPs at a DOX concentration of 0.1 µg/ml for 1 h. Then cells were rinsed thrice with cold PBS, fixed with 4% paraformaldehyde for 15 min, washed with 10% FBS (PBS, v/v) as blocking solution for 1 h and incubated with CD44 antibodies in blocking solution overnight at 4 °C. After this, cells were incubated with Rhodamine-labeled secondary antibodies for 1 h and stained with DAPI for 10 min. Confocal microscope was used to observe the images of samples.

2.6. Cytotoxicity

4T1 cells were seeded in 96-well plates at a density of 1×10^4 per well. After 24 h, cells were incubated with 100 µl free media containing varying concentrations of free DOX, BC-DOX-NPs, CS-DOX-NPs and blank carries for 24 or 48 h at 37 °C. The blank carries were prepared in the same way as the corresponding nanoparticles, but without DOX, and their added volume is equal to the corresponding nanoparticles. Afterward, the cells were incubated with 100 µl MTT (0.5 mg/ml) for 4 h at 37 °C and 150 µl dimethyl sulfoxide (DMSO) was added to develop color. The absorbance was recorded using a microplate reader at 490 nm. Cell viability was calculated using Eq. 1.

$$\text{Viability (\%)} = (A_{\text{text}} - A_{\text{blank}}) / (A_{\text{control}} - A_{\text{blank}}) \times 100\% \quad (1)$$

2.7. Biodistribution and tumor penetration

4T1 cells at a density of 2×10^6 per mouse were subcutaneously injected into the right flank of female balb/c mice weighting 18 ± 2 g. The experiment began when the tumor volume reached 200–500 mm³. Free DOX, CS-DOX-NPs and BC-DOX-NPs (5 mg/kg DOX) were administered intravenously via tail vein. After 1 and 4 h injection, the mice were sacrificed to collect major organs (heart, spleen, liver, lung and kidney) and tumor ($n=4$ per each group). These samples were weighted and homogenized with 3-fold of physiological saline (g/ml). The DOX in tissues was extracted with acetonitrile - methanol (5:1, v/v) and measured by LC-MS. In another set of experiment, after 5 min, 1 h and 4 h injection, the tumors were harvested and prepared for frozen sections. Tumors were fixed 4% paraformaldehyde, dehydrated with 20% and 40% sucrose in that order. After that the tumors were cryosectioned into 10 µm, then, cryosections were taken twice every 0.2 cm deep. The cryosections incubated with rabbit anti-CD31 antibodies in blocking solution overnight at 4 °C, and stained with Alexa Fluor 647 conjugated goat anti-rabbit IgG. Nuclei were stained with DAPI. The sections were observed by CLSM for tumor accumulation and penetration study.

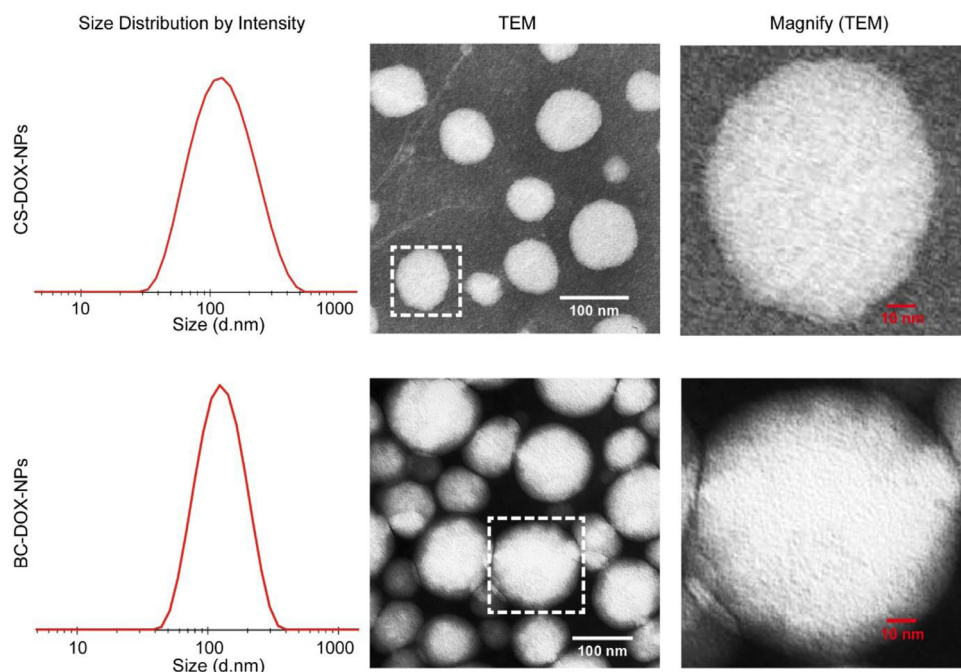


Fig. 2 – Size distributions and morphology of nanoparticles analyzed by DLS and TEM respectively. Unlike CS-DOX-NPs, BC-DOX-NPs has an extra translucent film with a thickness of about 10 nm.

2.8. *In vivo* antitumor efficacy

Balb/c mice (18 ± 2 g) bearing 4T1 breast tumor were established following the protocol described in biodistribution and divided into 4 groups randomly ($n = 8$). On the fourth day of inoculation, tumors reached $50\text{--}100\text{ mm}^3$ in volume and saline, free DOX, CS-DOX-NPs and BC-DOX-NPs were administered into mice intravenously at a dose of 5 mg/kg DOX every 4 d for three times. Tumor volume of each group was recorded after the first administration and calculated using Eq. 2.

$$\text{Volume}(\text{mm}^3) = \left[\text{length}(\text{mm}) \times \text{width}^2(\text{mm}) \right] / 2 \quad (2)$$

After 18 d of inoculation, the tumors were harvested from the mice and weighted to determined tumor inhibitory. Tumor inhibitory rate was calculated by following Eq. (3):

$$\text{Tumor inhibition rate} = (W_{\text{saline}} - W_{\text{drug}}) / W_{\text{saline}} \times 100\%. \quad (3)$$

2.9. Statistical analysis

All data are presented as mean with standard deviations (SD). Survival analysis was performed by SPSS software. *In vitro* release data were analyzed through the DDSolver program [26]. Statistical significance among groups were performed by ANOVA and a P value of < 0.05 was considered statistically significant.

3. Results and discussion

3.1. Preparation of CS-DOX-NPs and BC-DOX-NPs

When CS and DOX·HCl are dissolved in deionized water and stirred for a period of time, they can form nanoparticles directly without any additional materials. However, we found that the nanoparticles formed in this way easily dispersed after dilution. To increase their stability and entrapment, soybean oil, HS-15 and desalted DOX were added based on our previous studies [27]. Homogenization of soybean oil into a hydrophobic core helps DOX aggregate to form the positively charged core, which can combine with the negatively charged CS to form the desired CS-DOX-NPs (Fig. 2).

However, CS-DOX-NPs showed weak tumor targeting in our preliminary studies. Therefore, BSA was adsorbed onto the CS-DOX-NPs to generate a protein corona (Fig. 2), resulting in BC-DOX-NPs with improved tumor targeting ability. Meanwhile, the method of DOX·HCl desalting during preparation was simplified, and the feeding ratio of CS-to-DOX and the amounts of excipients and BSA were optimized (Fig. S1), to make our formulations closer to industrial applications. Meanwhile, we found that uniform nanoparticles could not form without the help of positively charged DOX (Fig. S2).

3.2. Properties of CS-DOX-NPs and BC-DOX-NPs

CS-DOX-NPs and BC-DOX-NPs were uniformly distributed nano-formulations with a particle size of approximately 100 nm (Table 1). The EE of BC-DOX-NPs slightly increased from 80.7% to 85.1% due to surface-coating BSA, compared

Table 1 – Characterization of CS-DOX-NPs and BC-DOX-NPs.

Groups	Particle size (nm)	PDI	Zeta potential (mV)	DL (%)	EE (%)
CS-DOX-NPs	99.71 ± 8.94	0.188 ± 0.02	-7.89 ± 0.65	9.34 ± 0.29	80.7 ± 1.2
BC-DOX-NPs	105.16 ± 13.15	0.173 ± 0.03	-3.52 ± 0.32	5.42 ± 0.14	85.1 ± 1.4

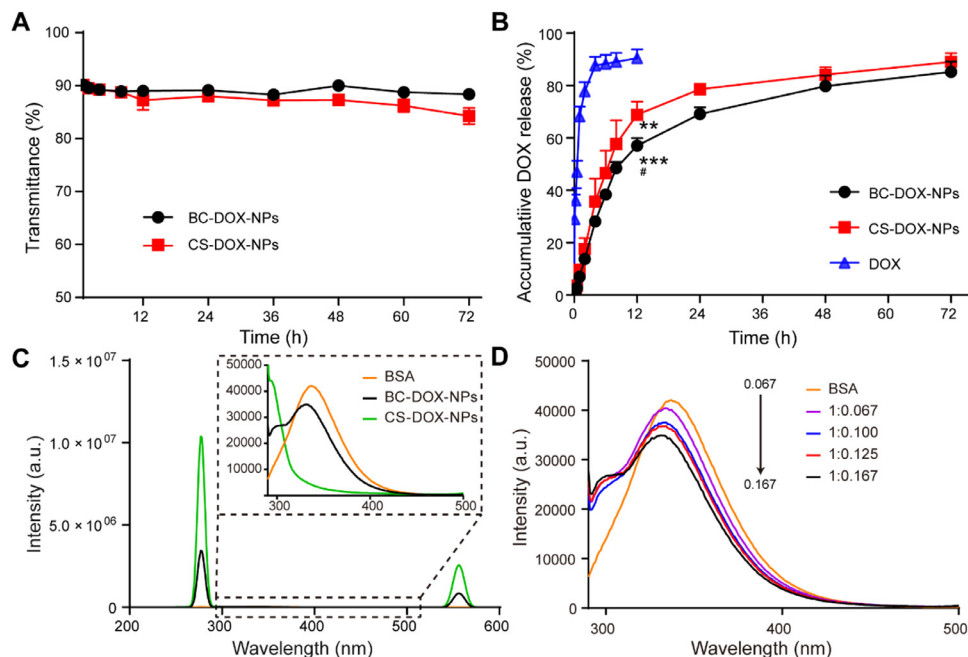


Fig. 3 – Properties of BC-DOX-NPs and CS-DOX-NPs. (A) Serum stability of BC-DOX-NPs and CS-DOX-NPs analyzed by transmittance when mixed in 50% FBS within a 72-h period (mean ± SD, n = 3). (B) In vitro release profiles of BC-DOX-NPs, CS-DOX-NPs and free DOX at 37 °C up to 72 h (mean ± SD, n = 3). **P < 0.01 and *P < 0.001 compared with free DOX; # P < 0.05 compared with CS-DOX-NPs. (C) Fluorescence emission spectra of BSA, BC-DOX-NPs and CS-DOX-NPs. Excitation wavelength: 280 nm. (D) Fluorescence emission spectra of BC-DOX-NPs with BSA/CS mass ratios of 1:0.167, 1:0.125, 1:0.100, 1:0.067. Excitation wavelength: 280 nm. (For interpretation of the references to colour in this figure legend, the reader is referred to the web version of this article.)**

to CS-DOX-NPs. Both formulations were stable during storage at 4 °C and 25 °C, and no increase in size or nanoparticle aggregation was observed under these conditions (Fig. S3). In serum, the transmittance of BC-DOX-NPs remained around 90% throughout the 72-h incubation (Fig. 3A), whereas that of CS-DOX-NPs began to decrease slightly after 24 h, implying that BC-DOX-NPs were more stable in serum.

In order to examine the effects of CS-DOX-NPs and BC-DOX-NPs on drug release, each formulation or free DOX was incubated in PBS for 72 h. At 6 h post-incubation, the cumulative release of free DOX was ~90%, while about 46% and 38% of the total drug was released from CS-DOX-NPs and BC-DOX-NPs, respectively (Fig. 3B). By 72 h, both formulations had released 90% of drug, indicating a sustained release effect. Furthermore, release was more sustained from BC-DOX-NPs than from CS-DOX-NPs (Fig. 3B and Table S1), as the release of DOX was blocked by the adsorbed BSA. The obtained data were then fitted using the DDSolver to analyze the release kinetics of BC-DOX-NPs. By comparing the goodness of fit of multiple dissolution models, we found that BC-DOX-NPs followed the Gompertz model with a regression

coefficient of 0.9970 and an Akaike information criterion of 44.60.

3.3. BSA fluorescence

Tryptophan ($\lambda_{ex} = 280$ nm) is the main endogenous fluorophore of BSA, allowing the use of fluorescence spectroscopy to analyze the stability of BSA or the effects of drugs on its structure [28,29]. CS-DOX-NPs did not interfere with the fluorescence of BSA (Fig. 3C). At the same concentration, the fluorescence intensity of BC-DOX-NPs was significantly lower than that of BSA, and a blue shift was observed at 290–500 nm (Fig. 3C); the CS-BSA interaction quenched BSA fluorescence. Comparison of the fluorescence intensity of BC-DOX-NPs and CS-DOX-NPs at λ_{max} of 271 and 556 nm further indicated that the adsorption of BSA on the surface reduced the fluorescence intensity of CS-DOX-NPs. Additionally, the fluorescence intensity of BC-DOX-NPs gradually decreased with increasing CS amount at a BSA concentration of 100 μ g/ml (Fig. 3D). All these results confirm that CS can interact with BSA, and that this interaction may be due to some positively charged

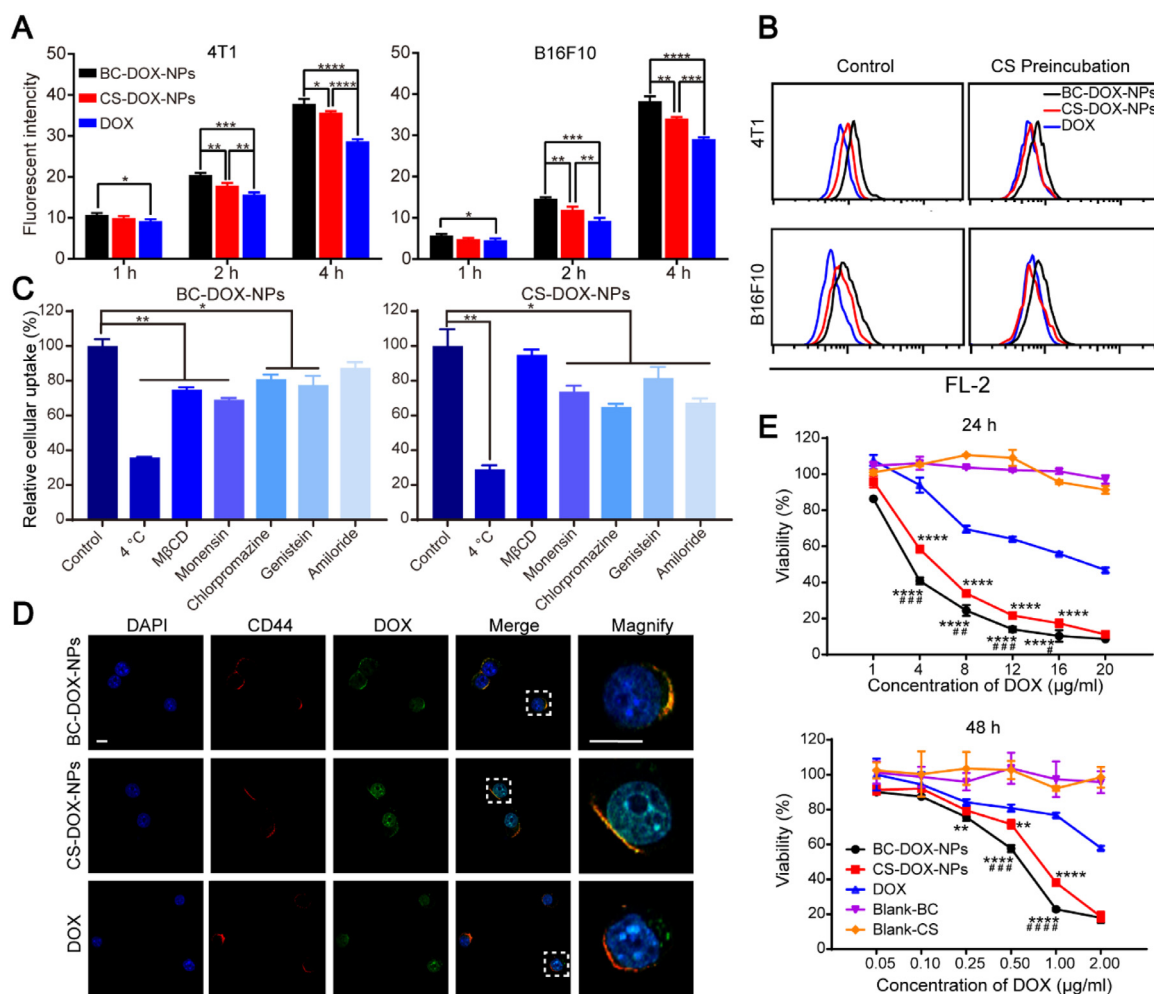


Fig. 4 – The in vitro cell-based experiments of formulations. (A) In vitro cellular uptake of BC-DOX-NPs, CS-DOX-NPs and free DOX in 4T1 cells and B16F10 cells after 1 h, 2 h and 4 h incubation, analyzed by flow cytometry. * $P < 0.05$, ** $P < 0.01$, * $P < 0.001$, **** $P < 0.0001$. (B) Flowcytometry histogram showing changes in cell uptake of BC-DOX-NPs and CS-DOX-NPs in 4T1 cells and B16F10 cells after preincubation with CS solution (10 mg/ml). (C) Relative uptake of BC-DOX-NPs and CS-DOX-NPs in 4T1 cells after preincubation with various cell uptake inhibitors, compared with control group. * $P < 0.05$, ** $P < 0.01$. (D) CLSM images of 4T1 cells incubated with BC-DOX-NPs, CS-DOX-NPs and free DOX for 1 h. The cell nuclei were stained by DAPI (blue). The CD44 receptors on 4T1 cells were stained by Rhodamine-labeled secondary antibodies (red). The fluorescence of DOX was shown in green and co-localization was shown in yellow. The bar is 10 µm. (E) Cytotoxicity of BC-DOX-NPs, CS-DOX-NPs, free DOX and blank carries in 4T1 cells after 24 h and 48 h incubation at different concentrations. All data represent mean \pm SD ($n = 3$). ** $P < 0.01$ and **** $P < 0.0001$ compared with free DOX; # $P < 0.05$, ## $P < 0.01$, ### $P < 0.001$, #### $P < 0.0001$ compared with CS-DOX-NPs. (For interpretation of the references to colour in this figure legend, the reader is referred to the web version of this article.)**

patches on BSA interacting with the negatively charged CS [30,31].

3.4. CD44-mediated cellular uptake of CS-DOX-NPs and BC-DOX-NPs

4T1 and B16F10 cells, which express abundant CD44, took up the prepared nano-formulations to a greater extent than they took up free DOX (Fig. 4A and Fig. S4), due to the CS wrapping, which promoted cell endocytosis via the CD44 receptor. Indeed, the BSA coating led BC-DOX-NPs to be taken up more efficiently than CS-DOX-NPs, suggesting that when

the CD44 receptors are saturated, tumor cells may endocytose nanoparticles by interacting with BSA. However, how BSA promotes uptake by cancer cells is still unclear; it may reflect that albumin serves as a nutrient for tumor cells, or it may result from increasing secretion of SPARC in the tumor microenvironment [17,32–34].

To further explore the effect of the CS-CD44 interaction on the cellular uptake of BC-DOX-NPs and CS-DOX-NPs, we preincubated the CD44-expressing cells with a CS solution for 1 h to block the CD44 receptors. Flow cytometry showed that the cellular uptake of BC-DOX-NPs and CS-DOX-NPs was significantly reduced (Fig. 4B). Nevertheless, the uptake of

BC-DOX-NPs remained higher than that of CS-DOX-NPs and free DOX. This suggests that although both formulations can be taken up by the cells via CD44-mediated endocytosis, BC-DOX-NPs also follow another endocytic pathway due to the BSA surface coating.

The intracellular distribution of formulations in CD44-expressing 4T1 cells was studied by confocal microscopy to verify their CD44 targeting ability. After incubation with free DOX for 1 h, the DOX (green) was mainly detected in the nucleus and randomly dispersed around it (Fig. 4D), and it did not overlap with the CD44 (labeled with red). In contrast, the fluorescence of DOX incorporated in CS-DOX-NPs and BC-DOX-NPs clearly overlapped with that of the CD44 receptor. Therefore, the presence of CS in both formulations promoted their ability to target the CD44 receptor on 4T1 cells. Interestingly, the fluorescence of DOX in BC-DOX-NPs was almost localized at the CD44 receptor sites, while that of CS-DOX-NPs was distributed mainly in the nucleus. This may be because CS-DOX-NPs are less stable than BC-DOX-NPs, so the DOX may have been released rapidly over time, allowing the drug to target the nucleus. Moreover, in contrast to the cellular uptake results, the fluorescence intensity of DOX in CS-DOX-NPs was higher than that in BC-DOX-NP. This is probably because the dose concentration of DOX was 0.1 µg/ml, which is significantly lower than that used in the cellular uptake experiments (5 µg/ml). The CD44 receptors were not saturated under these conditions and there are more CS on the CS-DOX-NPs, which allowing rapid uptake of CS-DOX-NPs.

3.5. Cellular uptake mechanism

To explore the mechanism of BC-DOX-NPs and CS-DOX-NPs uptake by 4T1 cells, internalization experiments were performed at 4 °C or in the presence of various inhibitors, including M-β-CD, an inhibitor of lipid raft/caveolae-dependent endocytosis; amiloride, an inhibitor of macropinocytosis-mediated endocytosis; chlorpromazine, an inhibitor of clathrin-mediated endocytosis; genistein, which inhibits caveolae-dependent endocytosis by reversibly inhibiting tyrosine kinase; and monensin, an inhibitor of microtubule-related endocytosis [35,36]. After incubation at 4 °C, the fluorescence intensity of BC-DOX-NPs and CS-DOX-NPs was considerably reduced, suggesting that their internalization is mediated by ATP-dependent endocytosis. In addition, most inhibitors inhibited the cellular uptake to varying degrees (Fig. 4C). Among them, M-β-CD and monensin had the strongest inhibitory effect on BC-DOX-NPs, while chlorpromazine and amiloride had the strongest inhibitory effect on CS-DOX-NPs. Based on these results, we conclude that the internalization of BC-DOX-NPs is mediated by lipid raft/caveolae and microtubule-dependent endocytosis, while CS-DOX-NPs are internalized via macropinocytosis and clathrin-mediated endocytosis.

3.6. Cytotoxicity

The cytotoxicity of the prepared formulations was examined in 4T1 cells incubated with various concentrations of free DOX, BC-DOX-NPs, or CS-DOX-NPs for 24 and 48 h. At the same

DOX concentrations, the targeting nanoparticles showed higher cytotoxicity against 4T1 cells than free DOX, and BC-DOX-NPs showed slightly higher cytotoxicity than CS-DOX-NPs (Fig. 4E). The IC₅₀ values of BC-DOX-NPs for 24 and 48 h were 5.3- and 4.4-fold lower, respectively, than the values of free DOX, while the corresponding IC₅₀ values of CS-DOX-NPs were 3.3- and 2.7-fold lower than those of free DOX (Table S2). Moreover, 4T1 cell viability was near 100% upon treatment with drug-free nanocarriers at various concentrations (Blank-BC and Blank-CS), indicating the high safety of the carriers. Thus, BC-DOX-NPs showed the greatest ability to inhibit proliferation of 4T1 cells, which is consistent with the cellular uptake results and suggests potential for breast cancer treatment.

3.7. Biodistribution and tumor penetration of CS-DOX-NPs and BC-DOX-NPs

To evaluate the biodistribution of DOX encapsulated in CS-DOX-NPs and BC-DOX-NPs, the major organs and tumor tissues of mice bearing 4T1 tumors were collected at 1 h and 4 h post-injection, and the DOX concentrations were quantitatively analyzed by LC-MS (Fig. 5A). At 1 and 4 h post-injection, DOX concentrations in the tumors of mice injected with BC-DOX-NPs were 1.4- and 2.7-fold higher than in the tumors of CS-DOX-NPs-injected mice, and 2.5- and 4.1-fold higher than in tumors of animals given free DOX. Interestingly, the accumulation of DOX in the heart was lower in the BC-DOX-NP-treated mice than in free DOX-treated mice, implying that the encapsulation reduces the cardiotoxicity of DOX.

Moreover, BC-DOX-NPs significantly reduced the drug concentration in the liver compared to CS-DOX-NPs. The increased accumulation of DOX in the liver of CS-DOX-NP-injected mice was mainly attributed to the reticuloendothelial system (RES) [37] and sinusoidal endothelial cells in liver. It has been reported that phagocytes in the RES can phagocytose particles by recognizing opsonins adsorbed on their surface [38,39]. However, the BSA on BC-DOX-NPs presumably inhibited such adsorption, limiting the accumulation of DOX in the mouse liver [40]. CS and hyaluronic acid (HA) were likely cleared systemically through interaction with the hyaluronic acid receptor for endocytosis (HARE), which is highly expressed on liver sinusoidal endothelial cells and is involved in endocytosis [41,42]. In contrast, the BSA coating reduced the ability of CS to target the liver.

To further examine drug penetration and accumulation in tumors, the tumor tissues of mice injected with formulations were harvested at 5 min, 1 h and 4 h post-injection and prepared as frozen sections. At 5 min post-injection, the fluorescence of DOX (green) and blood vessels (stained with anti-CD31 antibody, red) in the CS-DOX-NPs and free DOX groups overlapped slightly (Fig. 5B), whereas more extensive overlap was observed in the BC-DOX-NPs group, indicating the rapid passage of BC-DOX-NPs through the vascular endothelium. This significant difference could be attributed to the binding of BSA to gp60, which promoted the transcytosis of BC-DOX-NPs. In addition, at 1 h and 4 h post-injection, DOX penetrated and accumulated into the tumor tissues of both

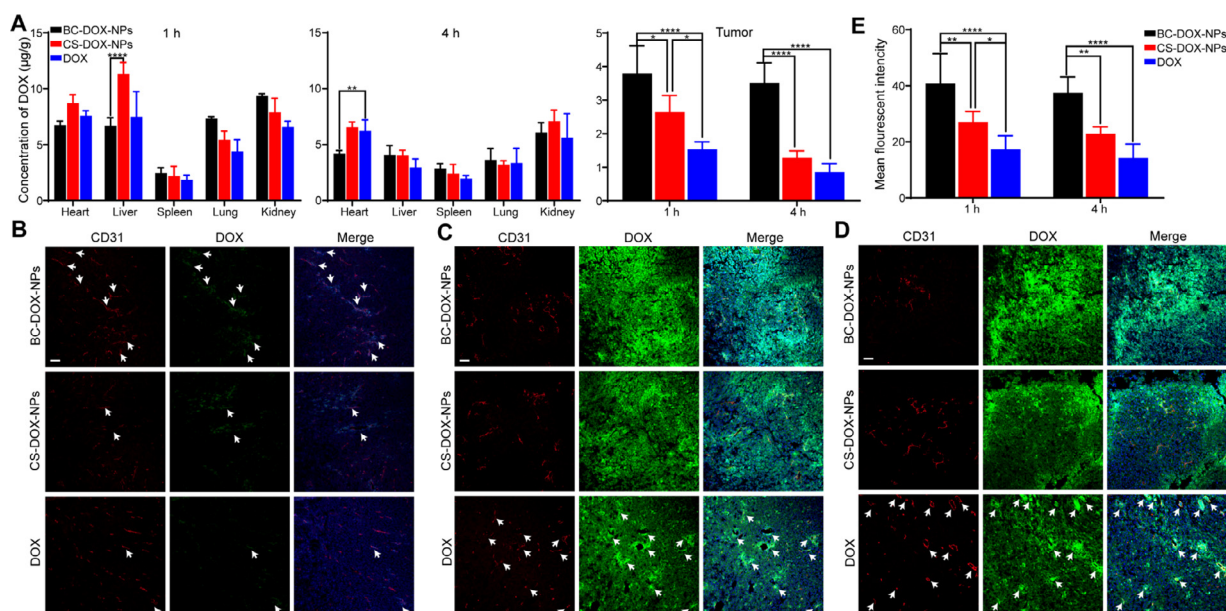


Fig. 5 – Biodistribution and tumor penetration of formulations. (A) The concentration of DOX in major organs and tumors of balb/c mice bearing 4T1 tumors after intravenous administration of BC-DOX-NPs, CS-DOX-NPs and free DOX at 1 h and 4 h. (mean \pm SD, $n = 4$). Distribution of BC-DOX-NPs, CS-DOX-NPs and free DOX in 4T1 tumors at (B) 5 min, (C) 1 h, and (D) 4 h post-injection. The tumor blood vessels are stained with anti-CD31 antibody (red) and nuclei are stained with DAPI (blue). The fluorescence of DOX was shown in green. The bar is 50 μ m. The white arrow points to the overlap between DOX and blood vessels. (E) The mean fluorescent intensity of DOX in tumors by semi-quantitative assessment. * $P < 0.05$, ** $P < 0.01$, **** $P < 0.0001$. (For interpretation of the references to colour in this figure legend, the reader is referred to the web version of this article.)

nanoparticle-treated groups (Fig. 5C and 5D), but to a greater extent in the BC-DOX-NPs group (Fig. 5E). In contrast, the drug in the free DOX group remained mainly around the blood vessels, showing no significant penetration. Similar results were observed at different depths of tumor sections (Fig. S5).

The LC-MS findings were consistent with the confocal imaging results. In particular, BC-DOX-NPs performed slightly better than CS-DOX-NPs *in vitro*, but the biodistribution of both formulations was significantly different *in vivo*. Active drug targeting and tumor accumulation by CS-DOX-NPs were due mainly to efficient targeting of CD44 and the EPR effect [1,43]. However, upon intravenous injection, the CS molecules on the nanoparticle surface could be shielded by opsonins, resulting in the more accumulation of nanoparticles to the liver. Therefore, BSA was pre-adsorbed onto the nanoparticle surface to form a protective protein corona, which could increase the stability in serum (Fig. 3C). In addition, BSA could bind to the gp60 receptor, favoring the rapid passage of BC-DOX-NPs through the vascular endothelial barrier, then their targeting of SPARC in tumors [44]. In other words, BC-DOX-NPs showed significantly greater tumor targeting and accumulation efficiency than CS-DOX-NPs *in vivo* due to the protective effect of BSA and the BSA-gp60-SPARC pathway.

3.8. Antitumor activity *in vivo*

The antitumor activity of the formulations was examined in female 4T1 tumor-bearing mice. The animals were divided into four groups (saline, free DOX, BC-DOX-NPs, and BC-DOX-

NPs). On Day 14 after the first treatment, mice were sacrificed, and their tumor tissues and major organs were harvested for further analysis. Results on tumor morphology, weight and growth inhibition are presented in Fig. 6B and 6C. The tumor volume was measured every 2 d as an indicator of the antitumor effect (Fig. 6A): the volumes in the free DOX, BC-DOX-NPs and BC-DOX-NPs groups were lower than that in the saline group by 49.2%, 62.0% and 82.8%, respectively. The tumor inhibition rate of BC-DOX-NPs was 91.4%, which was 1.5-fold higher than that of CS-DOX-NPs and 2.2-fold higher than that of free DOX. Moreover, the median survival of the BC-DOX-NPs-treated mice was 50 d, which was longer than that of groups treated with BC-DOX-NPs (43 d, $P < 0.05$), free DOX (38 d, $P < 0.01$), or saline (34 d, $P < 0.001$) (Fig. 6D and Table S2). Thus, while free DOX, CS-DOX-NPs and BC-DOX-NPs significantly inhibited tumor growth, BC-DOX-NPs showed the best treatment effect.

To further determine the antitumor efficacy of each group, the excised tumors were analyzed using histology and immunohistochemistry (Fig. 6E). H&E staining and TUNEL assays revealed the presence of a large necrotic and apoptotic region in the tumor tissues of the BC-DOX-NPs-treated mice, which was significantly larger than that in the other groups. The positive rate of antigen Ki-67 positively correlates with cell proliferation [45]. The number of Ki-67 positive cells in the BC-DOX-NPs group was significantly lower than that in the other groups (Fig. 6E), indicating that BC-DOX-NPs can efficiently inhibit cancer cell proliferation.

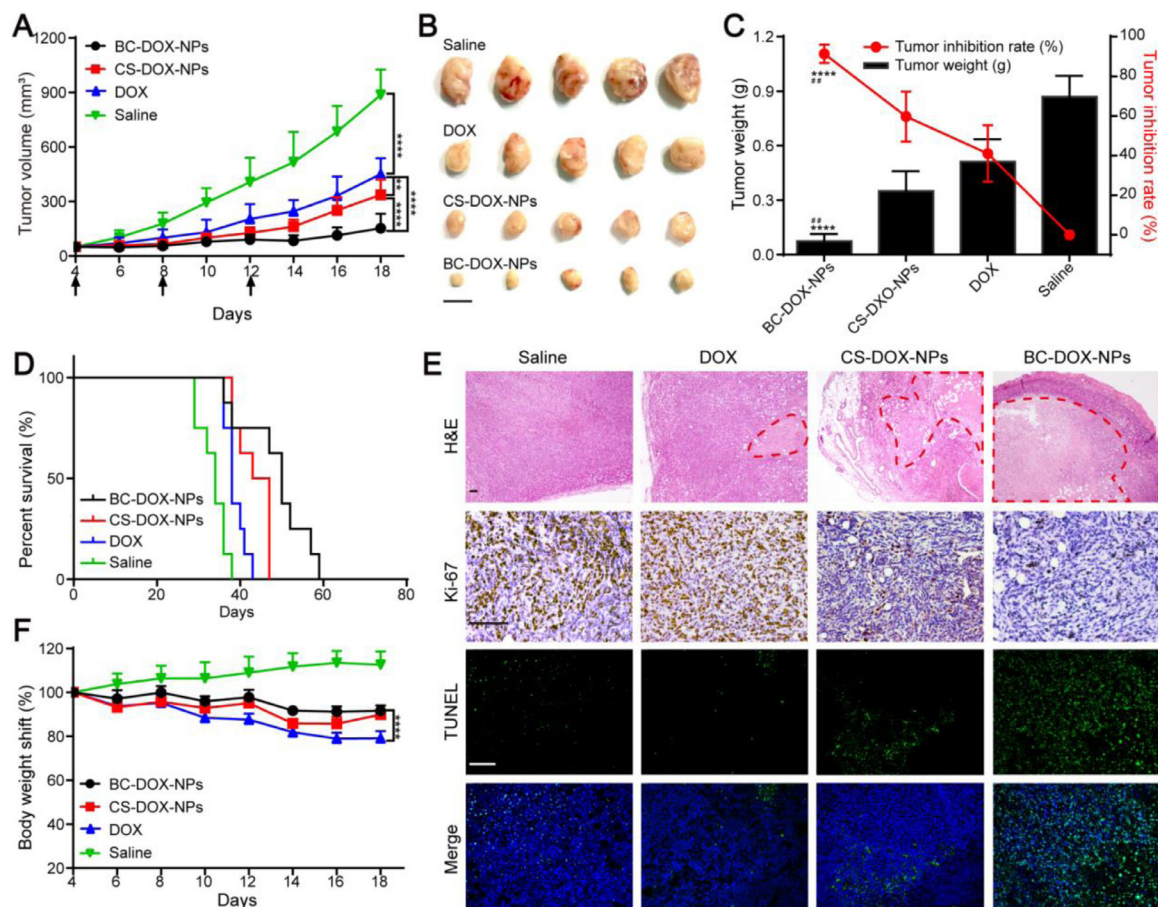


Fig. 6 – In vivo antitumor efficacy of formulations. (A) Mean tumor growth curves of mice bearing 4T1 tumors treated with saline, free DOX, CS-DOX-NPs and BC-DOX-NPs within 18 d after implantation. The arrows indicate the time of administration. (mean \pm SD, $n = 8$). $**P < 0.01$, $****P < 0.0001$. **(B)** Morphology of tumors harvested from treated mice at the end of the treatment. The black bar is 1 cm. **(C)** Tumor weight and tumor inhibition rate of treated mice at Day 18 post-implantation. (mean \pm SD, $n = 5$). $****P < 0.0001$ compared with free DOX; $## P < 0.01$ compared with CS-DOX-NPs. **(D)** The survival curves of mice bearing 4T1 tumors after administration with different formulations. (mean \pm SD, $n = 8$). **(E)** Histological and immunohistochemical analysis of 4T1 tumors slices by H&E (40 \times), Ki-67 (200 \times), and TUNEL (200 \times) staining at Day 18 post-implantation. The red dotted line represented the necrotic area in tumor tissue. The brown cells expressed as Ki-67 positive cells with high levels of tumor cell proliferation in the Ki-67 assay. Green fluorescence expressed as apoptotic cells in the TUNEL assay. The black and white bar is 100 μm . **(F)** Changes in body weight of treated mice during treatment. (mean \pm SD, $n = 8$). $**** P < 0.0001$. (For interpretation of the references to colour in this figure legend, the reader is referred to the web version of this article.)

H&E staining of the saline and free DOX groups revealed mild atrophy of myocardial fibers and obvious tumor metastases in the lungs, and the myocardial fibers in the BC-DOX-NPs group were autolyzed. In contrast, no obvious lesions were observed in the organs of the BC-DOX-NPs group (Fig. S6). Moreover, during the administration period, animal body weight in the BC-DOX-NPs group remained above 90% of the initial weight, while that in the free DOX group gradually decreased below 80% (Fig. 6F). These results showed that BC-DOX-NPs reduced the cardiotoxicity and systemic toxicity of DOX.

These *in vivo* results are consistent with previous *in vivo* and *in vitro* experimental results (Sections 3.4, 3.6 and 3.7). The drug encapsulated in BC-DOX-NPs was more efficiently

distributed into the tumor tissues than the drug delivered by CS-DOX-NPs, thereby reducing the exposure of other vital organs to DOX and enhancing antitumor effects.

4. Conclusion

In this study, we prepared two novel self-assembling nanoparticles encapsulating DOX without the use of chemical reactions or toxic chemicals. CS-DOX-NPs were formed based on positive and negative charge interactions, while BC-DOX-NPs were obtained via the adsorption of BSA on the BC-DOX-NPs surface. Both formulations displayed excellent stability and sustained release, effective CD44 targeting

and enhanced uptake by cells *in vitro*. However, BC-DOX-NPs performed better than CS-DOX-NPs *in vivo*, showing enhanced tumor specific distribution and penetration, which resulted in increased anticancer efficacy in a 4T1 mouse model. Our study reveals the potential of BC-DOX-NPs for active targeted tumor therapy, and their simple preparation may facilitate industrial applications as well.

Conflicts of interest

The authors have declared no conflict of interest.

Acknowledgments

Funding: This project was financially supported by grants from the National Natural Science Foundation of China (No. 81673359) and Sichuan Major Science and Technology Project on Biotechnology and Medicine (No. 2018SZDZX0018). Furthermore, Tiantian Tan wants to thank Qin Yang for her help and guidance in her studies and thoughts.

Supplementary materials

Supplementary material associated with this article can be found, in the online version, at doi:10.1016/j.ajps.2021.03.004.

REFERENCES

- [1] Afratis N, Gialeli C, Nikitovic D, Tsegenidis T, Karousou E, Theocharis AD, et al. Glycosaminoglycans: key players in cancer cell biology and treatment. *Febs J* 2012;279(7):1177–97.
- [2] Monzavi-Karbassi B, Stanley JS, Hennings L, Jousheghany F, Artaud C, Shaaf S, et al. Chondroitin sulfate glycosaminoglycans as major P-selectin ligands on metastatic breast cancer cell lines. *Int J Cancer* 2007;120(6):1179–91.
- [3] Liu Y, Yang H, Otaka K, Takatsuki H, Sakanishi A. Effects of vascular endothelial growth factor (VEGF) and chondroitin sulfate A on human monocytic THP-1 cell migration. *Colloids Surf B Biointerfaces* 2005;43(3–4):216–20.
- [4] Campoli M, Ferrone S, Wang XH. Functional and clinical relevance of chondroitin sulfate proteoglycan 4. *Adv Cancer Res* 2010;109:73–121.
- [5] Orian-Rousseau V. CD44, a therapeutic target for metastasising tumours. *Eur J Cancer* 2010;46(7):1271–7.
- [6] Zoller M. CD44: can a cancer-initiating cell profit from an abundantly expressed molecule? *Nat Rev Cancer* 2011;11(4):254–67.
- [7] Heldin P, Basu K, Kozlova I, Porsch H. HAS2 and CD44 in breast tumorigenesis. *Adv Cancer Res* 2014;123:211–29.
- [8] Liu C, Liu R, Zhang D, Deng Q, Liu B, Chao HP, et al. MicroRNA-141 suppresses prostate cancer stem cells and metastasis by targeting a cohort of pro-metastasis genes. *Nat Commun* 2017;8:14270.
- [9] Jing F, Kim HJ, Kim CH, Kim YJ, Lee JH, Kim HR. Colon cancer stem cell markers CD44 and CD133 in patients with colorectal cancer and synchronous hepatic metastases. *Int J Oncol* 2015;46(4):1582–8.
- [10] Pandey G, Mittapelly N, Banala VT, Mishra PR. Multifunctional glycoconjugate assisted nanocrystalline drug delivery for tumor targeting and permeabilization of lysosomal-mitochondrial membrane. *ACS Appl Mater Interfaces* 2018;10(20):16964–76.
- [11] Lee JY, Chung SJ, Cho HJ, Kim DD. Phenylboronic acid-decorated chondroitin sulfate A-based theranostic nanoparticles for enhanced tumor targeting and penetration. *Adv Funct Mater* 2015;25(24):3705–17.
- [12] Lundqvist M, Stigler J, Elia G, Lynch I, Cedervall T, Dawson KA. Nanoparticle size and surface properties determine the protein corona with possible implications for biological impacts. *P Natl Acad Sci USA* 2008;105(38):14265–70.
- [13] Peng Q, Zhang S, Yang Q, Zhang T, Wei XQ, Jiang L, et al. Preformed albumin corona, a protective coating for nanoparticles based drug delivery system. *Biomaterials* 2013;34(33):8521–30.
- [14] Chen X, Wang M, Hu Y, Gong T, Zhang ZR, Yu R, et al. Low-dose paclitaxel via hyaluronan-functionalized bovine serum albumin nanoparticulate assembly for metastatic melanoma treatment. *J Mater Chem B* 2020;8(10):2139–47.
- [15] Hu Y, Chen X, Xu Y, Han X, Wang M, Gong T, et al. Hierarchical assembly of hyaluronan coated albumin nanoparticles for pancreatic cancer chemoimmunotherapy. *Nanoscale* 2019;11(35):16476–87.
- [16] Guo L, Luo S, Du Z, Zhou M, Li P, Fu Y, et al. Targeted delivery of celastrol to mesangial cells is effective against mesangioproliferative glomerulonephritis. *Nat Commun* 2017;8(1):878.
- [17] Elzoghby AO, Samy WM, Elgindy NA. Albumin-based nanoparticles as potential controlled release drug delivery systems. *J Control Release* 2012;157(2):168–82.
- [18] Zhou Z, Zhang Q, Yang R, Wu H, Zhang M, Qian C, et al. ATP-charged nanoclusters enable intracellular protein delivery and activity modulation for cancer theranostics. *iScience* 2020;23(2):100872.
- [19] An FF, Zhang XH. Strategies for preparing albumin-based nanoparticles for multifunctional bioimaging and drug delivery. *Theranostics* 2017;7(15):3667–89.
- [20] Kudarha RR, Sawant KK. Albumin based versatile multifunctional nanocarriers for cancer therapy: fabrication, surface modification, multimodal therapeutics and imaging approaches. *Mater Sci Eng C Mater Biol Appl* 2017;81:607–626.
- [21] Stehle G, Sinn H, Wunder A, Schrenk HH, Stewart JCM, Hartung G, et al. Plasma protein (albumin) catabolism by the tumor itself - implications for tumor metabolism and the genesis of cachexia. *Crit Rev Oncol Hematol* 1997;26(2):77–100.
- [22] Ta HT, Dass CR, Larson I, Choong PFM, Dunstan DE. A chitosan-dipotassium orthophosphate hydrogel for the delivery of doxorubicin in the treatment of osteosarcoma. *Biomaterials* 2009;30(21):3605–13.
- [23] Mubaiwa TD, Hartley-Tassell LE, Semchenko EA, Day CJ, Jennings MP, Seib KL. The bexsero neisseria meningitidis serogroup B vaccine antigen NHBA is a high-affinity chondroitin sulfate binding protein. *Sci Rep* 2018;8(1):6512.
- [24] Papagiannopoulos A, Vlasi E. Stimuli-responsive nanoparticles by thermal treatment of bovine serum albumin inside its complexes with chondroitin sulfate. *Food Hydrocoll* 2019;87:602–10.
- [25] Papagiannopoulos A, Vlasi E, Radulescu A. Reorganizations inside thermally stabilized protein/polysaccharide nanocarriers investigated by small angle neutron scattering. *Carbohydr Polym* 2019;218:218–25.
- [26] Zhang Y, Huo M, Zhou J, Zou A, Li W, Yao C, et al. DDSolver: an add-in program for modeling and comparison of drug dissolution profiles. *AAPS J* 2010;12:263–71.

- [27] Li W, Yi X, Liu X, Zhang Z, Fu Y, Gong T. Hyaluronic acid ion-pairing nanoparticles for targeted tumor therapy. *J Control Release* 2016;225:170–82.
- [28] Saha A, Pradhan N, Chatterjee S, Singh RK, Trivedi V, Bhattacharyya A, et al. Fatty-amine-conjugated cationic bovine serum albumin nanoparticles for target-specific hydrophobic drug delivery. *ACS Appl Nano Mater* 2019;2(6):3671–83.
- [29] Lou YY, Zhou KL, Shi JH, Pan DQ. Characterizing the binding interaction of fungicide boscalid with bovine serum albumin (BSA): a spectroscopic study in combination with molecular docking approach. *J Photochem Photobiol B* 2017;173:589–597.
- [30] Khodarahmi R, Karimi SA, Ashrafi Kooshk MR, Ghadami SA, Ghobadi S, Amani M. Comparative spectroscopic studies on drug binding characteristics and protein surface hydrophobicity of native and modified forms of bovine serum albumin: possible relevance to change in protein structure/function upon non-enzymatic glycation. *Spectrochim Acta A Mol Biomol Spectrosc* 2012;89:177–86.
- [31] Chatterjee UR, Ray S, Micard V, Ghosh D, Ghosh K, Bandyopadhyay SS, et al. Interaction with bovine serum albumin of an anti-oxidative pectic arabinogalactan from *Andrographis paniculata*. *Carbohydr Polym* 2014;101:342–8.
- [32] Desai N, Trieu V, Yao Z, Louie L, Ci S, Yang A, et al. Increased antitumor activity, intratumor paclitaxel concentrations, and endothelial cell transport of cremophor-free, albumin-bound paclitaxel, ABI-007, compared with cremophor-based paclitaxel. *Clin Cancer Res* 2006;12(4):1317–24.
- [33] Schnitzer JE, Oh P. Antibodies to SPARC inhibit albumin binding to SPARC, gp60, and microvascular endothelium. *Am J Physiol* 1992;263:H1872–9.
- [34] Park CR, Jo JH, Song MG, Park JY, Kim YH, Youn H, et al. Secreted protein acidic and rich in cysteine mediates active targeting of human serum albumin in U87MG xenograft mouse models. *Theranostics* 2019;9(24):7447–57.
- [35] Gao G, Jiang YW, Sun W, Guo YX, Jia HR, Yu XW, et al. Molecular targeting-mediated mild-temperature photothermal therapy with a smart albumin-based nanodrug. *Small* 2019;15(33):e1900501.
- [36] Lv YQ, Xu CR, Zhao XM, Lin CS, Yang X, Xin XF, et al. Nanoplatform assembled from a CD44-targeted prodrug and smart liposomes for dual targeting of tumor microenvironment and cancer cells. *ACS Nano* 2018;12:1519–36.
- [37] Gref R, Minamitake Y, Peracchia MT, Trubetskoy V, Torchilin V, Langer R. Biodegradable long-circulating polymeric nanospheres. *Science* 1994;263:1600–3.
- [38] Liu D, Mori A, Huang L. Role of liposome size and RES blockade in controlling biodistribution and tumor uptake of GM1-containing liposomes. *Biochim Biophys Acta* 1992;1104(1):95–101.
- [39] Ernsting MJ, Murakami M, Roy A, Li SD. Factors controlling the pharmacokinetics, biodistribution and intratumoral penetration of nanoparticles. *J Control Release* 2013;172(3):782–94.
- [40] Ogawara K-i, Furumoto K, Nagayama S, Minato K, Higaki K, Kai T, et al. Pre-coating with serum albumin reduces receptor-mediated hepatic disposition of polystyrene nanosphere: implications for rational design of nanoparticles. *J Control Release* 2004;100(3):451–5.
- [41] Pandey MS, Harris EN, Weigel JA, Weigel PH. The cytoplasmic domain of the hyaluronan receptor for endocytosis (HARE) contains multiple endocytic motifs targeting coated pit-mediated internalization. *J Biol Chem* 2008;283(31):21453–61.
- [42] Harris EN, Weigel JA, Weigel PH. Endocytic function, glycosaminoglycan specificity, and antibody sensitivity of the recombinant human 190-kDa hyaluronan receptor for endocytosis (HARE). *J Biol Chem* 2004;279(35):36201–9.
- [43] Fang J, Nakamura H, Maeda H. The EPR effect: unique features of tumor blood vessels for drug delivery, factors involved, and limitations and augmentation of the effect. *Adv Drug Deliver Rev* 2011;63(3):136–51.
- [44] Kratz F. A clinical update of using albumin as a drug vehicle - a commentary. *J Control Release* 2014;190:331–6.
- [45] Inwald EC, Klinkhammer-Schalke M, Hofstadter F, Zeman F, Koller M, Gerstenhauer M, et al. Ki-67 is a prognostic parameter in breast cancer patients: results of a large population-based cohort of a cancer registry. *Breast Cancer Res Treat* 2013;139(2):539–52.